CHEMISTRY OF MATERIALS
Cite This: Chem. Mater. XXXX, XXX, XXX−XXX
Article
pubs.acs.org/cm

Understanding the Growth Mechanisms of Multilayered Systems in Atomic Layer Deposition Process

Christoph W. Wiegand,[†,‡] René Faust,[‡] Alexander Meinhardt,[‡] Robert H. Blick,[‡] Robert Zierold,[*,‡] and Kornelius Nielsch[†,§]

[†]Institute for Metallic Materials, Leibniz Institute for Solid State and Materials Research Dresden (IFW Dresden), Helmholtzstraße 20, 01069 Dresden, Germany

[‡]Center for Hybrid Nanostructures, Universität Hamburg, Luruper Chaussee 149, 22607 Hamburg, Germany

[§]Insitute of Material Science, Technical University Dresden, Helmholtzstraße 10, 01069 Dresden, Germany

Supporting Information

ABSTRACT: In atomic layer deposition (ALD), the initial growth is of particular interest because it defines the nucleation behavior and determines the minimum number of cycles to achieve a closed layer. The growth rate is quantified by the growth per cycle (GPC). Due to nucleation inhibition or enhancement, the initial GPC for ALD processes of a given material system onto a specific substrate may differ from its (steady-state) literature value because the GPC is mostly noted as an average value of at least a few hundred cycles. However, the knowledge of the growth behavior within the first few cycles is of particular importance in context of super cycles and nanolaminates. Individual ALD cycles of the host material (e.g., TiO_2) are replaced by those for the deposition of another compound (e.g., Al_2O_3) to infiltrate the host material with a dopant. For a precise dosage/doping and tailor-made synthesis, knowledge of the individual GPC is crucial. Herein, precise quartz crystal microbalance (QCM) studies were used to investigate the initial growth of TiO_2 onto Al_2O_3 (deposited by ALD) (1) and vice versa the initial growth of Al_2O_3 onto TiO_2 (2). In case 1, an enhanced initial GPC of the TiO_2 deposition was observed that was close to the equilibrium value of Al_2O_3 deposition. In the second case, the initial GPC of Al_2O_3 was found to be close to the equilibrium value of TiO_2 deposition. The growth process itself can be simply modeled by a superposition of parallel growth onto itself and onto the foreign species. We attribute our observations to an ALD process intrinsic inhibition of the TiO_2 growth.

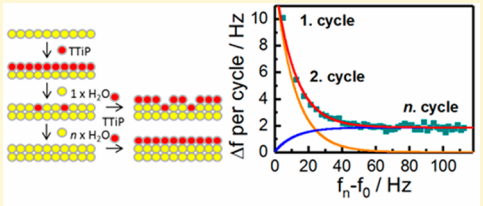

INTRODUCTION

The physical properties of thin films, such as surface roughness,[1] hardness,[2] lattice constant,[3] dielectric constant,[4] refractive index,[5] and phase-transition temperatures,[6] to name a few of them, mainly depend on their composition as well as crystallinity. The need for tailor-made materials whose properties are solely predetermined by external (working) conditions has risen with respect to economical and ecological usage of raw materials. For example, component parts of various devices and application areas are subjected to the most adverse environmental conditions during their use. A thermal barrier is essential for turbines, which work at temperatures up to 1650 °C to prevent the raw material from overheating and corrosion, elongating the turbine lifetime.[7] Novel promising approaches such as inverse titania opals, which act as photonic crystals in the near-infrared, lack structural stability at temperatures higher than 1000 °C, mostly due to crystallization and loss of microstructure.[8] The use of dual material systems such as nanolaminates or by doping can shift the phase-transition temperature to higher temperatures, making the inversed opals much more stable at elevated temperatures.[6,9] Hence, the preparation method of choice has to be versatile, capable of processing various materials and material combinations and able to produce a conformal coating. Specifically, atomic layer deposition (ALD) is one method which enables the experimentalist to synthesize multilayer systems by utilizing supercycle approaches.[10] In detail, through adjustment of the number of ALD cycles of the combined (two or more) individual processes according to the known growth rates, the synthesis of tailor-made ternary materials is possible in addition to doping of a specific species into a host material. A wide variety of novel, tailor-made, composite materials has been employed utilizing ALD methods, including alloys,[3,11−23] nanolaminates,[5,24−32] doped materials,[33−37] and mixed oxides.[38,39] For multilayer systems as well as nanolaminates with individual layer thicknesses in the lower nm-range, corresponding to at least several tenths of ALD cycles, the individual layers and thus the total film growth can be described by the equilibrium growth rates. However, the depicted deposition behavior of one material onto the surface of the host material becomes important when ALD is used for doping of only a small amount of material into a host or into extremely thin layers. As a proof-of-concept, we herein investigate the interplay of the first pulses of Al_2O_3 and TiO_2 depositions onto each

Received: December 10, 2017
Revised: February 17, 2018
Published: February 23, 2018

DOI: 10.1021/acs.chemmater.7b05128
Chem. Mater. XXXX, XXX, XXX−XXX

other and show that surface-dependent inhibition can be observed which may drastically alter the physical properties of compounds deposited by a supercycle approach.

EXPERIMENTAL SECTION

General ALD Deposition Parameters. A QCM from Colnatec was modified to fit into an in-house built ALD reaction chamber for measuring the change in frequency, which corresponds to a change in mass. The depositions were conducted using continuous flow mode by utilizing trimethylaluminum (TMA) (Sigma-Aldrich) and DI water at room temperature and titanium tetrakis isopropoxide ($Ti(O^iPr)_4$) (Sigma-Aldrich) heated to 85 °C as precursors. The pulse times corresponds to 0.4 s (TMA), 0.4 s (H_2O), and 2 s ($Ti(O^iPr)_4$), respectively. The purge time was kept between 60 s (after the metal-precursor pulses) and 90 s (after the H_2O pulses) for the general depositions. The pulse lengths and purge times were chosen based on results in growth studies in the exposure mode[40−42] and according to literature.[43,44] The flow of Ar(5.0) carrier gas was set to 2.5 l/h.

Deposition of Alternating Al_2O_3 and TiO_2 Thin Films. A sequential deposition of 50 cycles TiO_2 onto prior deposited TiO_2 and 50 cycles of Al_2O_3 onto prior deposited Al_2O_3 served as reference. In the following, the growth of 50 cycles TiO_2 (Al_2O_3) was analyzed as a function of the number n (m) of ALD cycles of the prior deposited material, namely Al_2O_3 (TiO_2). The experimental procedure is schematically sketched in Figure 1a.

Influence of Purging Time on TiO_2 Growth Behavior. The time between individual blocks of 30 TiO_2 ALD cycles was varied between 300 and 7200 s, and the initial growth of the subsequent cycle was observed. A schematic sketch is shown in Figure 1b.

Validation Experiment with Multiple H_2O Pulses onto a TiO_2 Surface. A TiO_2 thin film deposited by 50 cycles of $Ti(O^iPr)_4$ and H_2O was treated within 1 h with 2−40 H_2O pulses (2, 4, 8, 16, 20, or 40). The variation in frequency of the following TiO_2 deposition, especially during the first cycle, was measured.

RESULTS AND DISCUSSION

We utilized a quartz crystal microbalance (QCM) setup which possesses a resolution high enough to differentiate between the single pulses of each precursor used in the ALD deposition process.[1,45] The resonance frequency of the QCM changes with additionally deposited mass onto the crystal. A typical frequency pattern during an ALD deposition of $Ti(O^iPr)_4$ + H_2O onto previously deposited TiO_2 is shown in Figure 2a.

The stepwise variation of the frequency corresponds to $Ti(O^iPr)_4$ as well as H_2O pulses, which is read as mass (ng/cm^2) deposition during each of the individual pulses. By calculating the slope of such a curve, it is possible to identify the growth rate of the deposited material. The high resolution in

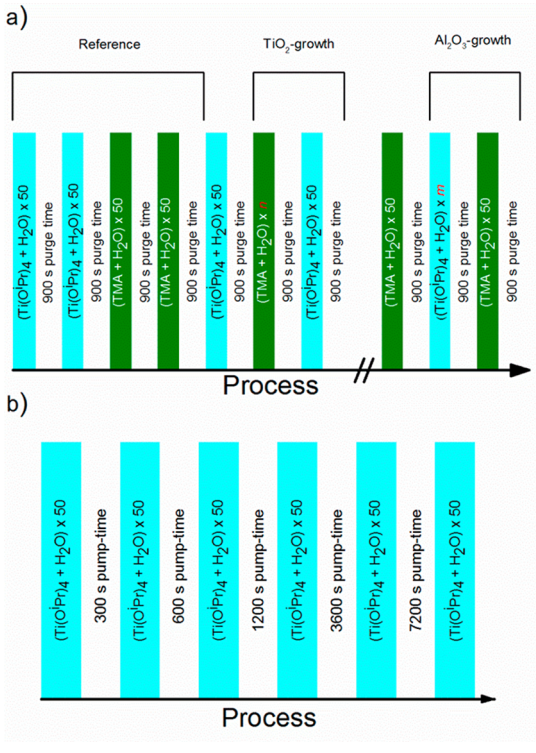

Figure 1. (a) Schematic illustration of the ALD cycles. TiO_2 and Al_2O_3 were deposited onto themselves, separated with 900 s purging time, as a reference, whereas the further growth of TiO_2 and Al_2O_3 was performed on top of previously deposited Al_2O_3 and TiO_2, respectively. (b) Schematic illustration of deposition cycles of TiO_2 (blue) separated by blocks (highlighted in white) with varying purging time.

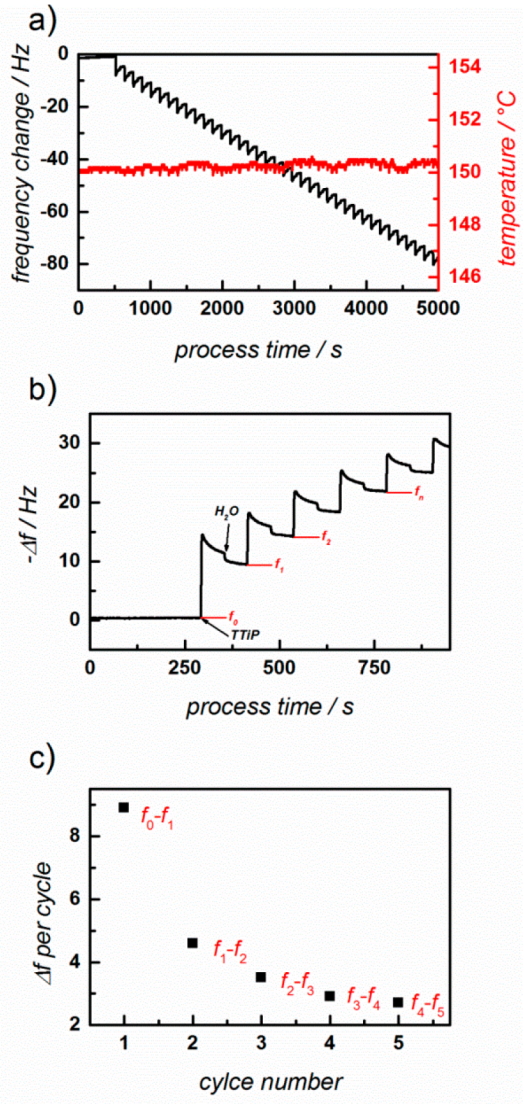

Figure 2. (a) Frequency variation (black) and temperature (red) during a $Ti(O^iPr)_4$ + H_2O process recorded by a QCM. (b) Negative frequency variation for the first few pulses of $Ti(O^iPr)_4$ + H_2O onto an Al_2O_3 surface as a function of process time. (c) Influence of previous Al_2O_3 cycle(s) on the frequency variation during the following deposition of TiO_2.

DOI: 10.1021/acs.chemmater.7b05128
Chem. Mater. XXXX, XXX, XXX−XXX

frequency and time of the QCM setup permits the study of only a few ALD cycles onto different surfaces. For depositing TiO_2 onto itself (which is shown in Figure 2a, the first pulse has the same variation of frequency, corresponding to a mass uptake of about Δf = ~2 Hz/cycle, as the following pulses, indicating a negligible influence of the surface onto the first pulses and leading to a constant growth rate over the entire process. The same applies to the deposition of Al_2O_3 from TMA and H_2O (see Supporting Information, Figure S1) onto an Al_2O_3 surface with a frequency change of Δf = ~9 Hz/cycle. Conversely, when the surface is changed from previously deposited TiO_2 to previously deposited Al_2O_3, the first pulses of $Ti(O^iPr)_4$ + H_2O differ dramatically in amplitude from the following ones, which is displayed in Figure 2b. To ease the comparison of the frequency variation during TiO_2 cycles ($Ti(O^iPr)_4$ + H_2O), the frequency before the first pulse is named f_0 and the frequencies after the nth cycle as f_n (e.g., f_1 after the first cycle, f_2 after the second cycle etc.). The change in frequency, corresponding to the mass uptake during the cycle, is then obtained from $\Delta f_n = f_{n-1} - f_n$. The negative change in frequency is plotted in Figure 2b; due to the inversely proportional correlation of the frequency and mass of the crystal, ascending curve reveals a mass uptake and therefore film growth. The gained frequency variation during the first pulses of $Ti(O^iPr)_4$ + H_2O is plotted in Figure 2c: Δf_n decreases from the first cycle with approximately 9 Hz down to already approximately 4.5 Hz during the second cycle and continues to decrease below 3 Hz. This trend points to the conclusion that the first cycles of TiO_2 deposition onto an Al_2O_3 surface lead to a mass deposition higher than the deposition onto a TiO_2 surface. This difference of deposition behavior, reflected in the mass gain, can only be explained by the different surfaces presented to the gaseous precursors. As demonstrated previously by Kim et al.,[46] no reaction between TMA and $Ti(O^iPr)_4$ is expected, hinting to a general difference in growth behavior of the surfaces of TiO_2 and Al_2O_3.

To further investigate the influence of different surfaces or modifications of the surfaces, a variable amount of Al_2O_3 pulses was deposited in between two TiO_2 depositions, and the frequency variation during the first 50 cycles was observed for each block. The frequency variation per pulse is depicted in Figure 3. The inset in Figure 3a displays the frequency variation when a variable amount of Al_2O_3 layers is deposited in between two blocks of TiO_2 depositions. The change in frequency of each TiO_2 cycle for 1, 2, 4, and 8 cycles of prior Al_2O_3 deposition is presented in Figure 3a. The effect of a higher mass deposition rate caused by the prior Al_2O_3 deposition vanishes after approximately 10 cycles of TiO_2 deposition. However, for the first few pulses (<10), the TiO_2 growth is greatly affected, especially Δf of the first cycle, and increases drastically with an increasing number of prior Al_2O_3 cycles. When only focusing on the first cycle of the further TiO_2 deposition, it is clear that even one single cycle of Al_2O_3 already has a significant influence on the sequential growth of TiO_2, leading to an increase in Δf. Furthermore, with increasing cycle numbers of prior deposited Al_2O_3, the frequency variation is elevated up to more than five times when in comparison with a steady state TiO_2 deposition. Depicted in Figure 3b is the normalized Δf for the first cycle of TiO_2 deposition depending on n cycle(s) of previously deposited Al_2O_3 (left) and the normalized Δf for the first cycle of Al_2O_3 deposition depending on m cycle(s) of previously deposited TiO_2 (right).

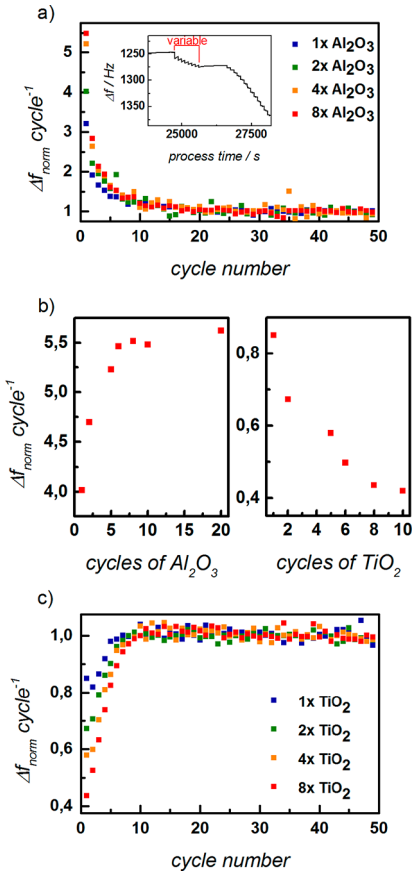

Figure 3. (a) Normalized frequency variation during the deposition of TiO_2 after previous depositions of 1, 2, 4, and 8 cycles of Al_2O_3. The inset demonstrates an overview of the conducted experiment and a change in frequency during the deposition of Al_2O_3 and the following deposition of TiO_2. The change in frequency is normalized to the equilibrium change in frequency during a normal deposition of TiO_2. (b) The influence of the numbers of previous Al_2O_3 cycles on the frequency variation during the first pulse of TiO_2 deposition (left); frequency variation during the first pulse of Al_2O_3 deposition after different numbers of TiO_2 cycles (right). (c) The frequency variation according to the cycle number during the deposition of Al_2O_3 after the previous deposition of 1, 2, 4, and 8 cycles of TiO_2.

It is obvious that with a sufficient number of Al_2O_3 cycles, to form a closed layer of Al_2O_3 deposited in between, the frequency variation during the first TiO_2 cycle reaches a maximum value of mass deposition, which is approximately five times as high as that during a steady state growth of TiO_2. This effect of increased mass deposition seems to be almost independent of the temperature (compare data of Figure 3 b) deposited at 95 °C and Figure S2 (Supporting Information, deposited at 150 °C) which shows the same trend.

In contrast, by depositing Al_2O_3 subsequently to m previously deposited cycles of TiO_2, a reduced frequency variation, and therefore mass deposition, in the beginning was observed. As depicted in Figure 3c, the initial inhibiting influence of the previously deposited TiO_2 vanishes after a certain amount of Al_2O_3 cycles, and the overall deposition rate reaches a constant equilibrium value, though the first few cycles show a frequency variation which is much lower than that during the normal growth of Al_2O_3. Again, this effect was found to be independent of the temperature (compare data of Figure

DOI: 10.1021/acs.chemmater.7b05128
Chem. Mater. XXXX, XXX, XXX−XXX

3b) deposited at 95 °C and Figure S3 (Supporting Information) deposited at 150 °C).

Note, the conducted experiments demonstrate that the underlying material plays an important role for the deposition of both materials. Additionally, the frequency variation of the first pulses for a TiO_2 deposition onto an Al_2O_3-covered surface is increased up to a value, which is in the range of the frequency variation during the general deposition of Al_2O_3 onto itself; conversely, the frequency variation during the first cycle of Al_2O_3 deposition onto an TiO_2 covered surface is decreased to a value, which is comparable to that of TiO_2 onto itself.

The authors want to emphasize that, for validation of the given results the frequency variation of a completed pulse was considered and no kinetic considerations by analyzing the time course of the frequency variation were made.

For elaboration of a model to calculate the actual growth rate of one of the discussed materials, the ratio of surface groups in dependence of the amount of cycles has to be taken into account.

Starting with a surface formed by depositing Al_2O_3, the surface is terminated with Al_2O_3 surface species ($SS(Al_2O_3)$), functioning as anchor groups for the following $Ti(O^iPr)_4$ precursor. This surface apparently enables for a higher mass deposition compared to a TiO_2 surface ($SS(TiO_2)$). The first cycle of $Ti(O^iPr)_4 + H_2O$ partially covers the Al_2O_3 surface, introducing $SS(TiO_2)$ as new anchor groups. As mentioned, the reaction onto a $SS(Al_2O_3)$ seems to enable for a higher mass deposition than on a $SS(TiO_2)$. After introduction of the first $SS(TiO_2)$ onto the surface, the following $Ti(O^iPr)_4 + H_2O$ pulses see both surface species. With increasing number of $Ti(O^iPr)_4 + H_2O$ cycles, the $SS(Al_2O_3)$ get completely covered by $SS(TiO_2)$ and are not accessible for further cycles. Expressed differently, the previous Al_2O_3 surface is converted into a TiO_2 surface gradually with each cycle. On the basis of this simple model, one can think of a combination of both surfaces with depending mass deposition rates adding up to a total growth rate in dependence of the (initial) ratio of surface species. Specifically, for the growth of TiO_2, we have two different conditions: first, the growth onto an $SS(Al_2O_3)$

$$G^{TiO_2}_{SS(Al_2O_3)} = Ae^{(-f_n - f_0)/\beta} \quad (1)$$

and second the growth onto $SS(TiO_2)$

$$G^{TiO_2}_{SS(TiO_2)} = C_{TiO_2} - (C_{TiO_2} - B)e^{(-f_n - f_0)/\beta} \quad (2)$$

where the frequency variations $C_{Al_2O_3}$ and C_{TiO_2} correspond to the frequency variations per cycle of Al_2O_3 and TiO_2 deposited onto itself and are independent of the conducted experiment. This definition holds true for the default deposition sequences with a pulse ratio of the organometallic precursors and water of 1:1. The expression $f_n - f_0$ equals to the difference in frequency after the nth cycle subtracted by the start frequency, as described in Figure 2b). A and B are defined as the surface coverage dependent frequency variations per cycle onto the surface species $SS(Al_2O_3)$ and $SS(TiO_2)$, respectively.

$$A = \frac{n_{Al_2O_3}}{n_{Al_2O_3} + n_{TiO_2}} C_{Al_2O_3} \text{ and } B = \frac{n_{TiO_2}}{n_{Al_2O_3} + n_{TiO_2}} C_{TiO_2} \quad (3)$$

The combination of eqs 1−3 result in an overall growth per cycle behavior of TiO_2 depending on the ratio of surface species:

$$GPC^{TiO_2} = C_{TiO_2} + \frac{n_{Al_2O_3}}{n_{Al_2O_3} + n_{TiO_2}} (C_{Al_2O_3} - C_{TiO_2}) e^{(-f_n - f_0)/\beta} \quad (4)$$

By fitting the given results with this equation, we determined β, which is a relaxation term, and equal to 12.5 ± 1.5 Hz. This relaxation term is a technical constant, which describes the change in frequency necessary to achieve saturation of all $SS(Al_2O_3)$ with the precursor $Ti(O^iPr)_4$ and which is independent of the amount of previously deposited Al_2O_3 cycles. Thus, the model only depends on the ratio between TiO_2- and Al_2O_3-surface groups, which varies due to the amount of previously deposited Al_2O_3. Exemplarily, the frequency-dependent growth behavior of TiO_2 after six cycles of previously deposited Al_2O_3 is shown in Figure 4 a), where

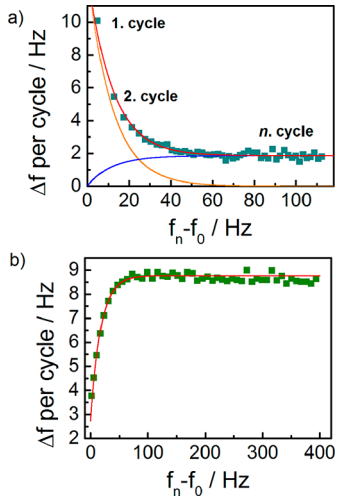

Figure 4. Frequency variation per cycle according to the overall frequency variation during the deposition of (a) TiO_2 and (b) Al_2O_3. The data points show the deposition of TiO_2 after six cycles of previous deposited Al_2O_3 (blue data points) and of Al_2O_3 after eight cycles of previous deposited TiO_2 (green data points). The red lines correspond to the applied model, while the blue line and the orange line represent the deposition onto Al_2O_3 surface species and the deposition onto TiO_2 surface species, respectively.

the measured data points (blue squares) and the resulting fit of the model (red curve) are compared. Additionally, the two individual contributions $G^{TiO_2}_{SS(Al_2O_3)}$ and $G^{TiO_2}_{SS(TAiO_2)}$ are plotted in orange and blue curves, respectively. After a change in frequency of $f_n - f_0 \sim 50$ Hz, the influence of the Al_2O_3 surface species vanishes, which means that no further Al_2O_3 surface species are accessible for further growth, and the normal growth rate of TiO_2 onto itself is established.

For the deposition of Al_2O_3 onto TiO_2, the definition of the growth behavior onto both surface species is analogous:

$$G^{Al_2O_3}_{SS(TiO_2)} = Be^{(-f_n - f_0)/\gamma} \quad (5)$$

for the growth of Al_2O_3 onto $SS(TiO_2)$ and

$$G^{Al_2O_3}_{SS(Al_2O_3)} = C_{Al_2O_3} - (C_{Al_2O_3} - A)e^{(-f_n - f_0)/\gamma} \quad (6)$$

for the growth onto a $SS(Al_2O_3)$. The overall growth per cycle behavior of Al_2O_3 depending on the ratio of surface species is obtained from the combination of eqs 5, 6, and 3:

$$GPC^{Al_2O_3} = C_{Al_2O_3} - \frac{n_{TiO_2}}{n_{Al_2O_3} + n_{TiO_2}} (C_{Al_2O_3} - C_{TiO_2}) e^{(-f_n - f_0)/\gamma} \quad (7)$$

DOI: 10.1021/acs.chemmater.7b05128
Chem. Mater. XXXX, XXX, XXX−XXX

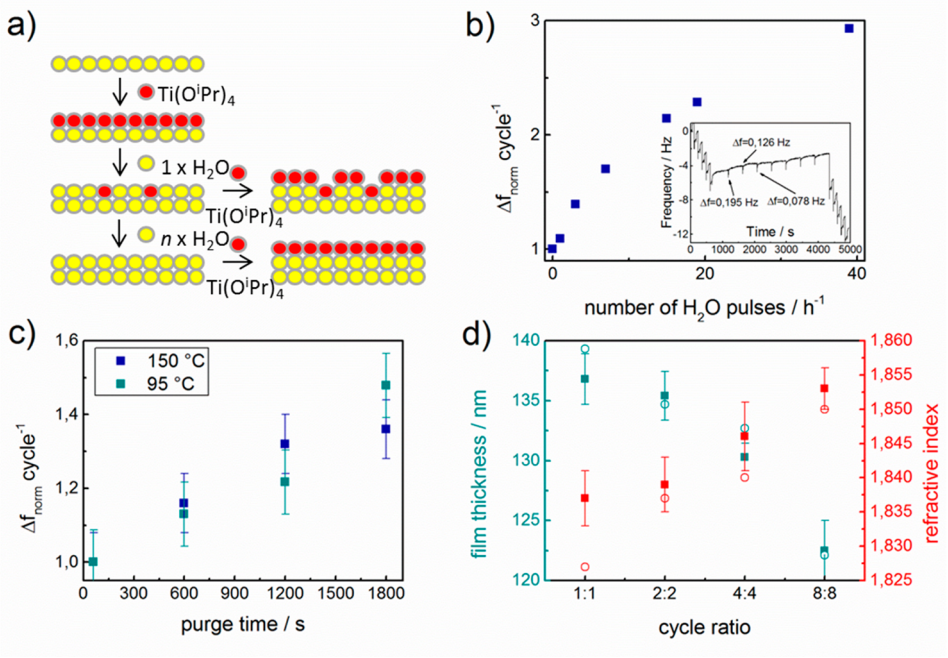

Figure 5. (a) Schematic illustration of the inhibition model during the deposition of TiO_2 and the nullification of the inhibition due to multiple H_2O pulses. (b) Frequency variation during the first pulse of a TiO_2 deposition after the previous treatment with several H_2O pulses; the inset demonstrates the observed change in frequency during the introduction of (eight) pulses of H_2O. (c) Frequency variation during the first pulse of a TiO_2 deposition after elongated purge times at temperatures of 95 °C (light blue) and 150 °C (dark blue). (d) The combination of 1600 cycles on total of TiO_2 and Al_2O_3 with different ratios and the resulting film thicknesses (blue) and refractive indexes (red). The experimental data correspond to the solid squares; the fitted data applying the presented model correspond to the hollow circles.

By fitting the given results with this equation, we were able to determine the relaxation term γ to be 17.6 ± 2.3 Hz. The effect of eight previously deposited cycles of $Ti(O^iPr)_4$ + H_2O onto an Al_2O_3 deposition is presented in Figure 4b exemplarily. The green squares represent the data points, and the resulting fit of the model is depicted as the red curve.

Our applied model is in good agreement for the measured growth behaviors. After determining the technical constants β and γ, the model is able to describe the growth behavior of Al_2O_3 onto TiO_2 and vice versa according to the surface-groups ratio. Thus, the experimentalist is enabled to forecast the growth of these two materials onto each other, which is essential for a correct calculation of stoichiometry for the fabrication of doped samples or thin multilayer systems as well as thin cover layers.

Nonetheless, the general observation that the amount of deposited mass during the first pulses of both materials depends only on the underlying surface and its ratio of surface groups, leading to the conclusion that the general difference in growth rate between the deposition of Al_2O_3 and the deposition of TiO_2 is due to a growth inhibition during the ALD growth of TiO_2. An etching mechanism as seen in the deposition of aluminum doped zinc oxide (AZO) can be excluded because no mass loss is observed during the TiO_2 treatment with TMA.[45,47] Because the growth during the first pulse of Al_2O_3 onto a previously deposited TiO_2 surface shows the same behavior as TiO_2 onto itself, we assume that the inhibition is caused by the $Ti(O^iPr)_4$ precursor. The used precursors are well-established in ALD because of their self-limiting character.[48] After the first pulse of the $Ti(O^iPr)_4$ precursor, the originally −OH terminated surface is now terminated with $-O^iPr$ groups. These surface groups are self-limiting to both $Ti(O^iPr)_4$ and TMA respectively. Nevertheless, the following ALD half cycle introducing H_2O to the surface is supposed to react with those surface groups to convert the surface again into −OH species and lead to an desorption of isopropanol molecules as described in literature.[49−51] However, Hoffmann et al.[52] showed that this reaction step is only limited by the chemical reaction rate and that a small amount of $-O^iPr$ stays unreacted on the surface after the water pulse. The remaining unreacted $-O^iPr$ species act than as an inhibitor because the self-limiting character still remains during the following $Ti(O^iPr)_4$ or TMA pulse. This behavior requires the elongation or multiple repetition of the water pulse to promote a complete reaction of the surface.[52] A generalized scheme is depicted in Figure 5a, demonstrating the inhibiting effect of unreacted $-O^iPr$ groups during the pulse of H_2O in comparison with n repetitions of H_2O pulses to promote a complete surface reaction. The nonreacted $-O^iPr$ groups can be considered as an intrinsic inhibitor for the subsequent growth of either TiO_2 or Al_2O_3. As mentioned earlier, the presence of unreacted $-O^iPr$ groups at the surface leads to an overall inhibited mass deposition during one cycle of TiO_2 deposition. This mass deposition, measured as frequency variation, was defined as C_{TiO_2} within the model. Modifying the surface species due to multiple H_2O pulse leads to a modification of C_{TiO_2}, which then has to be considered during the application of the presented model. The authors want to emphasize that the model was applied to a deposition process including a pulse ratio of the organometallic precursors and water of 1:1, as it is used in default ALD processes.

The characteristics of isopropanol as a growth inhibitor in ALD processes has been previously reported by the Elam group.[53] However, in contrast to the general model of process inhibition, the remaining isopropoxide groups are not

DOI: 10.1021/acs.chemmater.7b05128
Chem. Mater. XXXX, XXX, XXX−XXX

introduced separately to cover the surface partially beforehand; instead, the inhibitor arises from the previous reaction, leading to a general intrinsic inhibition during the growth of TiO_2 by means of $Ti(O^iPr)_4$ and H_2O as precursors. Additionally, this inhibition characteristic remains even during the pulse of TMA as shown in this work, which differs from the behavior observed when using $TiCl_4$ as precursor for TiO_2.[54] The departure of a chlorine group of the precursor $TiCl_4$ is facilitated, which can lead to an additional uptake of TMA onto an already saturated surface treated with $TiCl_4$.[54] The usage of $Ti(O^iPr)_4$ as precursor does not enable such a side reaction and is therefore preferred as a self-limiting ALD precursor.

To validate the model, multiple numbers of H_2O pulses in the time period of 1 h have been introduced onto a surface of a deposited TiO_2 film and the change in frequency has been monitored. As depicted in the inlet of Figure 5b, the introduction of H_2O leads to a decrease in mass, which is magnified by further water pulses.

This behavior can be attributed to the hydrolysis of remaining isopropyl groups to hydroxyl groups on the surface, which leads to a secession of the heavier isopropyl groups reflected as an overall mass loss. The surface gets sequentially converted into a Ti−OH terminated interface, leading to a mass loss, which of course results in an increased mass uptake behavior during the following first pulse, as depicted in Figure 5b due to an increased amount of ALD-active surface groups. It is obvious that after applying a sufficient amount of water pulses, a frequency variation and therefore mass uptake during the first pulse is achieved, which is comparable to the growth onto a pure Al_2O_3 surface. This observation validates the previous assumption that the reason behind the lower growth onto a TiO_2 surface is due to an intrinsic inhibition mechanism. An altered deposition cycle with elongated H_2O pulse times would result in an increased growth per cycle (for detailed change in growth rate in dependence of the individual pulse times, see Supporting Information, Figures S4−S7). With H_2O pulse times exceeding the above applied 0.4 s during the deposition of TiO_2, an increased growth rate was observed. Especially with H_2O pulse times exceeding 1 s, a highly increased growth per cycle was determined. This is in good agreement with previous results of Sinha et al.,[55] which showed an increase in growth rate with H_2O pulse times up to 2.5 s. Within the conducted experiment, pulse times up to 5 s were applied, demonstrating a strong variation of the growth rate in dependence of the H_2O pulse times. According to the assumed intrinsic inhibition, a longer pulse time leads to a higher amount of hydrolyzed O^iPr groups and a lower inhibition during the subsequent growth. In detail, growth rates of 0.003 Å/cycle up to 1.0 Å/cycle have been reported for the deposition of TiO_2 utilizing the same precursors.[48,50,51,55−67,44,68−76,43]

Because we did not use an ultrahigh vacuum system or ultrapure carrier gas, an absence of water in the purge gas or in the chamber could not be achieved completely because traces of humidity might have been introduced into the chamber through small leakages or impurities of the purge gas. The presence of H_2O was verified by a control experiment by pulsing highly reactive TMA solely into the chamber. A small, but measurable growth of 0.04 Å/pulse was observed.

Hence, a long pump time also leads to a small but measurable decrease in mass due to continuous hydrolysis of the remaining isopropoxyl groups on the surface. Figure 5c shows the normalized frequency variation during the first pulse of a TiO_2 deposition onto an ALD deposited TiO_2 surface, which was purged for various time periods beforehand. The frequency variation during the first pulse is increased when an extended purge time is applied between two blocks of TiO_2 depositions. This effect points to a continuous hydrolysis of remaining isopropoxyl groups which effectively counteracts the intrinsic inhibition. The theoretical limitation would be a complete hydrolyses to achieve an OH terminated surface. By comparing the OH coverages of TiO_2 with 12−14 OH/nm^2[77] and Al_2O_3 with ∼15 OH/nm^2,[78] a mass deposition of comparable amounts for both surfaces can be expected.

However, the OH coverages are the theoretical maximum values; both materials show a reduction in OH coverages in experimental analyses due to bare Ti, Al, and O sites on the surface.[77,78] Because the observed reduction is in the same order for both materials, the difference in OH coverage seems to be negligible small. Furthermore, no significant temperature dependence was found. As mentioned previously, the inhibition effect can be traced back to the presented surface groups and can be correlated to their different chemical reactivity between them and the gaseous precursors.

In summary, an intrinsic inhibition process was identified, and a model was developed to fit the observed growth behaviors under consideration of different surface species and their influence on the mass deposition rate. As depicted in Figure 5d, the model enables a more accurate calculation of the combined deposition of two materials with each other. The calculated layer thicknesses and refractive indexes in terms of an effective medium model fit very well with the experimental results and demonstrate that the applied model describes the observed inhibited growth process quite well.

Additional experiments were conducted to show the influence of a high H_2O concentration on a freshly deposited TiO_2 layer over time by an elongated purge time or multiple H_2O pulses. With this, it was possible to suppress the intrinsic inhibition during the TiO_2 deposition. The wide range of previously reported growth rates for the deposition process of TiO_2 corroborates the importance of a well-known surface composition. This indicates that the identified intrinsic inhibition process may have caused such a variety of growth rates.

With respect to generality, one can argue that the class of metal-alkoxide ALD precursors may suffer from a process-dependent intrinsic inhibition caused by an incomplete release of alcohols. This possibility gives hint that only an introduction of a higher amount of H_2O due to longer pulse times, longer purge times, or multiple pulses of H_2O can increase the growth rate by overcoming the intrinsic inhibition. Alternatively, the usage of ozone may also overcome the intrinsic inhibition because the not so well-controlled decomposition process of the isopropyl groups would open other reaction pathways in the ALD process. It was already shown that with the use of ozone and more elevated temperatures, no inhibition in the deposition of TiO_2 was observed.[79]

Finally, we would like to point out that care has to be taken by deposition of nanolaminates or compound materials because a simple combination of two (or more) well-established processes might end up with unintended results regarding stoichiometry and film thickness. However, the knowledge of shown intrinsic inhibition mechanisms leads to the development of model systems, as demonstrated above, which enables the manufacturer for exact calculations of pulse ratio to get the desired doping level and compound stoichiometry.

DOI: 10.1021/acs.chemmater.7b05128
Chem. Mater. XXXX, XXX, XXX−XXX

■ ASSOCIATED CONTENT

Supporting Information

The Supporting Information is available free of charge on the ACS Publications website at DOI: 10.1021/acs.chemmater.7b05128.

Temperature comparison of the growth of TiO_2 onto various cycles of Al_2O_3, temperature comparison of the growth of Al_2O_3 onto various cycles of TiO_2, growth per cycle in dependence of the individual precursor pulse times for TiO_2 and Al_2O_3 (PDF)

■ AUTHOR INFORMATION

Corresponding Author

*E-mail: rzierold@physik.uni-hamburg.de.

ORCID

Christoph W. Wiegand: 0000-0001-5644-3415

Robert Zierold: 0000-0003-0292-0970

Author Contributions

C.W.W., R.Z., and K.N. conceived the idea for the project. C.W.W., R.F., and A.M. performed the ALD processes as well as QCM studies with the support of R.Z. All authors analyzed the results. C.W.W. and R.Z. wrote the manuscript with substantial contribution from all authors. R.H.B., R.Z., and K.N. supervised the project. All authors have given approval to the final version of the manuscript.

Funding

This work was supported by the German Research Foundation (DFG) through the SFB 986.

Notes

The authors declare no competing financial interest.

■ ACKNOWLEDGMENTS

The authors want to thank Dr. Kaline Furlan for proofreading and useful discussion.

■ REFERENCES

(1) Elam, J. W.; Sechrist, Z. A.; George, S. M. ZnO/Al2O3 Nanolaminates Fabricated by Atomic Layer Deposition: Growth and Surface Roughness Measurements. *Thin Solid Films* **2002**, *414* (1), 43−55.

(2) Chu, X.; Wong, M. S.; Sproul, W. D.; Barnett, S. A. Deposition, Structure, and Hardness of Polycrystalline Transition-Metal Nitride Superlattice Films. *J. Mater. Res.* **1999**, *14* (6), 2500−2507.

(3) Fujiwara, H.; Nabeta, T.; Shimizu, I. Structures and Properties of (ZnS)n(ZnSe)m(n = 1−4) Ordered Alloys Grown by Atomic Layer Epitaxy. *Jpn. J. Appl. Phys.* **1994**, *33* (Part 1, No. 5A), 2474−2478.

(4) Strømme, M.; Niklasson, G. A.; Ritala, M.; Leskelä, M.; Kukli, K. Ta1-xNbx)2O5 Films Produced by Atomic Layer Deposition: Temperature Dependent Dielectric Spectroscopy and Room-Temperature I-V Characteristics. *J. Appl. Phys.* **2001**, *90* (9), 4532−4542.

(5) Kattelus, H.; Ylilammi, M.; Saarilahti, J.; Antson, J.; Lindfors, S. Layered Tantalum-Aluminum Oxide Films Deposited by Atomic Layer Epitaxy. *Thin Solid Films* **1993**, *225* (1−2), 296−298.

(6) Rodríguez-Talavera, R.; Vargas, S.; Arroyo-Murillo, R.; Montiel-Campos, R.; Haro-Poniatowski, E. Modification of the Phase Transition Temperatures in Titania Doped with Various Cations. *J. Mater. Res.* **1997**, *12* (2), 439−443.

(7) Kelly, M. J.; Wolfe, D. E.; Singh, J.; Eldridge, J.; Zhu, D. M.; Miller, R. Thermal Barrier Coatings Design with Increased Reflectivity and Lower Thermal Conductivity for High-Temperature Turbine Applications. *Int. J. Appl. Ceram. Technol.* **2006**, *3* (2), 81−93.

(8) Rudisill, S. G.; Wang, Z.; Stein, A. Maintaining the Structure of Templated Porous Materials for Reactive and High-Temperature Applications. *Langmuir* **2012**, *28* (19), 7310−7324.

(9) Furlan, K. P.; Krekeler, T.; Ritter, M.; Blick, R.; Schneider, G. A.; Nielsch, K.; Zierold, R.; Janßen, R. Low-Temperature Mullite Formation in Ternary Oxide Coatings Deposited by ALD for High-Temperature Applications. *Adv. Mater. Interfaces* **2017**, *4*, 1−8.

(10) Kukli, K.; Ihanus, J.; Ritala, M.; Leskela, M. Tailoring the Dielectric Properties of HfO2-Ta2O5 Nanolaminates. *Appl. Phys. Lett.* **1996**, *68* (26), 3737−3739.

(11) Strømme, M.; Niklasson, G. A.; Ritala, M.; Leskelä, M.; Kukli, K. (Ta[sub 1−x]Nb[sub X])[sub 2]O[sub 5] Films Produced by Atomic Layer Deposition: Temperature Dependent Dielectric Spectroscopy and Room-Temperature I−V Characteristics. *J. Appl. Phys.* **2001**, *90* (9), 4532.

(12) Juppo, M.; Alén, P.; Ritala, M.; Leskelä, M. Trimethylaluminum as a Reducing Agent in the Atomic Layer Deposition of Ti(Al)N Thin Films. *Chem. Vap. Deposition* **2001**, *7* (5), 211−217.

(13) Schuisky, M.; Kukli, K.; Ritala, M.; Hårsta, A.; Leskelä, M. Atomic Layer CVD in the Bi−Ti−O System. *Chem. Vap. Deposition* **2000**, *6* (3), 139−145.

(14) Song, J. H.; Sim, E. D.; Baek, K. S.; Chang, S. K. Optical Properties of ZnSxSe1−x (x < 0.18) Random and Ordered Alloys Grown by Metalorganic Atomic Layer Epitaxy. *J. Cryst. Growth* **2000**, *214−215*, 460−464.

(15) Vehkamäki, M.; Hatanpää, T.; Hänninen, T.; Ritala, M.; Leskelä, M. Growth of SrTiO3 and BaTiO3 Thin Films by Atomic Layer Deposition. *Electrochem. Solid-State Lett.* **1999**, *2* (10), 504−506.

(16) Nilsen, O.; Peussa, M.; Fjellvåg, H.; Niinistö, L.; Kjekshus, A. Thin Film Deposition of Lanthanum Manganite Perovskite by the ALE Process. *J. Mater. Chem.* **1999**, *9* (8), 1781−1784.

(17) Seim, H.; Mölsä, H.; Nieminen, M.; Fjellvåg, H.; Niinistö, L. Deposition of LaNiO3 Thin Films in an Atomic Layer Epitaxy Reactor. *J. Mater. Chem.* **1997**, *7* (3), 449−454.

(18) Seim, H.; Nieminen, M.; Niinistö, L.; Fjellvåg, H.; Johansson, L.-S. Growth of LaCoO3 Thin Films from β-Diketonate Precursors. *Appl. Surf. Sci.* **1997**, *112*, 243−250.

(19) Ihanus, J.; Ritala, M.; Leskelä, M.; Rauhala, E. ALE Growth of ZnS1−xSex Thin Films by Substituting Surface Sulfur with Elemental Selenium. *Appl. Surf. Sci.* **1997**, *112*, 154−158.

(20) Boutros, K. S.; McIntosh, F. G.; Roberts, J. C.; Bedair, S. M.; Piner, E. L.; El-Masry, N. A. High Quality InGaN Films by Atomic Layer Epitaxy. *Appl. Phys. Lett.* **1995**, *67* (13), 1856−1858.

(21) Asikainen, T.; Ritala, M.; Leskela, M. Growth of Indium-Tin-Oxide Thin Films by Atomic Layer Epitaxy. *J. Electrochem. Soc.* **1995**, *142* (10), 3538−3541.

(22) Fujiwara, H.; Nabeta, T.; Kiryu, H.; Shimizu, I. Preparation and Properties of (ZnS)3(ZnSe)42 Ordered Alloys Fabricated by Plasma-Enhanced Low-Temperature Growth Technique. *Jpn. J. Appl. Phys.* **1994**, *33* (7B), 4381−4384.

(23) McDermott, B. T.; Reid, K. G.; El-Masry, N. A.; Bedair, S. M.; Duncan, W. M.; Yin, X.; Pollak, F. H. Atomic Layer Epitaxy of GaInP Ordered Alloy. *Appl. Phys. Lett.* **1990**, *56* (12), 1172−1174.

(24) Kukli, K.; Ritala, M.; Leskelä, M. Properties of Atomic Layer Deposited (Ta1−xNbx)2O5 Solid Solution Films and Ta2O5−Nb2O5 Nanolaminates. *J. Appl. Phys.* **1999**, *86* (10), 5656−5662.

(25) Zhang, H.; Solanki, R. Atomic Layer Deposition of High Dielectric Constant Nanolaminates. *J. Electrochem. Soc.* **2001**, *148* (4), F63−F66.

(26) Kukli, K.; Ritala, M.; Leskelä, M. Development of Dielectric Properties of Niobium Oxide, Tantalum Oxide, and Aluminum Oxide Based Nanolayered Materials. *J. Electrochem. Soc.* **2001**, *148* (2), F35−F41.

(27) Zhang, H.; Solanki, R.; Roberds, B.; Bai, G.; Banerjee, I. High Permittivity Thin Film Nanolaminates. *J. Appl. Phys.* **2000**, *87* (4), 1921−1924.

(28) Kumagai, H.; Toyoda, K.; Kobayashi, K.; Obara, M.; Limura, Y. Titanium Oxide/aluminum Oxide Multilayer Reflectors for "water-Window" Wavelengths. *Appl. Phys. Lett.* **1997**, *70* (18), 2338−2340.

DOI: 10.1021/acs.chemmater.7b05128
Chem. Mater. XXXX, XXX, XXX−XXX

(29) Ishii, M.; Iwai, S.; Kawata, H.; Ueki, T.; Aoyagi, Y. Atomic Layer Epitaxy of AlP and Its Application to X-Ray Multilayer Mirror. *J. Cryst. Growth* **1997**, *180* (1), 15−21.
(30) Hartmann, J. M.; Charleux, M.; Mariette, H.; Rouvière, J. L. Atomic Layer Epitaxy of CdTe, MgTe and MnTe; Growth of CdTe/MnTe Tilted Superlattices on Vicinal Surfaces. *Appl. Surf. Sci.* **1997**, *112*, 142−147.
(31) Kukli, K.; Ihanus, J.; Ritala, M.; Leskela, M. Tailoring the Dielectric Properties of HfO2-Ta2O5 Nanolaminates. *Appl. Phys. Lett.* **1996**, *68* (26), 3737−3739.
(32) Ritala, M.; Leskelä, M.; Niinistö, L.; Prohaska, T.; Friedbacher, G.; Grasserbauer, M. Surface Roughness Reduction in Atomic Layer Epitaxy Growth of Titanium Dioxide Thin Films. *Thin Solid Films* **1994**, *249* (2), 155−162.
(33) Yousfi, E. B.; Weinberger, B.; Donsanti, F.; Cowache, P.; Lincot, D. Atomic Layer Deposition of Zinc Oxide and Indium Sulfide Layers for Cu(In,Ga)Se2 Thin-Film Solar Cells. *Thin Solid Films* **2001**, *387* (1−2), 29−32.
(34) Jung, D.; Leonard, M.; El-Masry, N. E.; Bedair, S. M. Selenium Doping of GaInP by Atomic Layer Epitaxy. *J. Electron. Mater.* **1995**, *24* (2), 75−78.
(35) Elers, K.-E.; Ritala, M.; Leskelä, M.; Rauhala, R. NbCl5 as a Precursor in Atomic Layer Epitaxy. *Appl. Surf. Sci.* **1994**, *82-83*, 468−474.
(36) Kong, W.; Fogarty, J.; Solanki, R. Atomic Layer Epitaxy of ZnS:Tb Thin Film Electroluminescent Devices. *Appl. Phys. Lett.* **1994**, *65* (6), 670−672.
(37) Viirola, H.; Niinistö, L. Controlled Growth of Antimony-Doped Tin Dioxide Thin Films by Atomic Layer Epitaxy. *Thin Solid Films* **1994**, *251* (2), 127−135.
(38) Nieminen, M.; Sajavaara, T.; Rauhala, E.; Putkonen, M.; Niinistö, L. Surface-Controlled Growth of LaAlO3 Thin Films by Atomic Layer Epitaxy. *J. Mater. Chem.* **2001**, *11* (9), 2340−2345.
(39) Haukka, S.; Lindblad, M.; Suntola, T. Growth Mechanisms of Mixed Oxides on Alumina. *Appl. Surf. Sci.* **1997**, *112*, 23−29.
(40) Furlan, K. P.; Pasquarelli, R. M.; Krekeler, T.; Ritter, M.; Zierold, R.; Nielsch, K.; Schneider, G. A.; Janssen, R. Highly Porous α-Al2O3ceramics Obtained by Sintering Atomic Layer Deposited Inverse Opals. *Ceram. Int.* **2017**, *43* (14), 11260−11264.
(41) Kubrin, R.; Pasquarelli, R. M.; Waleczek, M.; Lee, H. S.; Zierold, R.; Do Rosário, J. J.; Dyachenko, P. N.; Montero Moreno, J. M.; Petrov, A. Y.; Janssen, R.; Eich, M.; Nielsch, K.; Schneider, G. A. Bottom-up Fabrication of Multilayer Stacks of 3D Photonic Crystals from Titanium Dioxide. *ACS Appl. Mater. Interfaces* **2016**, *8* (16), 10466−10476.
(42) Pasquarelli, R. M.; Lee, H. S.; Kubrin, R.; Zierold, R.; Petrov, A. Y.; Nielsch, K.; Schneider, G. A.; Eich, M.; Janssen, R. Enhanced Structural and Phase Stability of Titania Inverse Opals. *J. Eur. Ceram. Soc.* **2015**, *35* (11), 3103−3109.
(43) Doring, H.; Hashimoto, K.; Fujishima, A. TiO2 Thin Films Prepared by Pulsed Beam Chemical Vapor Deposition from Titanium Tetraisopropoxide and Water. *Ber. Bunsenges. Phys. Chem. 96* **1992**, *96* (4), 620−622.
(44) Ritala, M.; Leskelä, M.; Niinistö, L.; Haussalo, P. Titanium Isopropoxide as a Precursor in Atomic Layer Epitaxy of Titanium Dioxide Thin Films. *Chem. Mater.* **1993**, *5* (8), 1174−1181.
(45) Groner, M. D.; Fabreguette, F. H.; Elam, J. W.; George, S. M. Low-Temperature Al2O3 Atomic Layer Deposition. *Chem. Mater.* **2004**, *16* (4), 639−645.
(46) Kim, S. K.; Choi, G.-J.; Hwang, C. S. Controlling the Composition of Doped Materials by ALD: A Case Study for Al-Doped TiO2 Films. *Electrochem. Solid-State Lett.* **2008**, *11* (7), G27−G29.
(47) Elam, J. W.; Routkevitch, D.; George, S. M. Properties of ZnO/Al2O3 Alloy Films Grown Using Atomic Layer Deposition Techniques. *J. Electrochem. Soc.* **2003**, *150* (6), G339−G347.
(48) Miikkulainen, V.; Leskelä, M.; Ritala, M.; Puurunen, R. L. Crystallinity of Inorganic Films Grown by Atomic Layer Deposition: Overview and General Trends. *J. Appl. Phys.* **2013**, *113* (213001), 1−101.
(49) Ritala, M.; Leskelä, M.; Niinistö, L.; Haussalo, P. Titanium Isopropoxide as a Precursor in Atomic Layer Epitaxy of Titanium Dioxide Thin Films. *Chem. Mater.* **1993**, *5* (8), 1174−1181.
(50) Rahtu, A.; Ritala, M. Reaction Mechanism Studies on Titanium Isopropoxide−Water Atomic Layer Deposition Process. *Chem. Vap. Deposition* **2002**, *8* (1), 21−28.
(51) Aarik, J.; Aidla, A.; Uustare, T.; Ritala, M.; Leskelä, M. Titanium Isopropoxide as a Precursor for Atomic Layer Deposition: Characterization of Titanium Dioxide Growth Process. *Appl. Surf. Sci.* **2000**, *161* (3), 385−395.
(52) Reinke, M.; Kuzminykh, Y.; Hoffmann, P. Surface Reaction Kinetics of Titanium Isopropoxide and Water in Atomic Layer Deposition. *J. Phys. Chem. C* **2016**, *120* (8), 4337−4344.
(53) Yanguas-Gil, A.; Libera, J. A.; Elam, J. W. Modulation of the Growth Per Cycle in Atomic Layer Deposition Using Reversible Surface Functionalization. *Chem. Mater.* **2013**, *25* (24), 4849−4860.
(54) Arroval, T.; Aarik, L.; Rammula, R.; Kruusla, V.; Aarik, J. Growth of TixAl1−xOy Films by Atomic Layer Deposition Using Successive Supply of Metal Precursors. *Thin Solid Films* **2016**, *600*, 119−125.
(55) Sinha, A.; Hess, D. W.; Henderson, C. L. Area Selective Atomic Layer Deposition of Titanium Dioxide: Effect of Precursor Chemistry. *J. Vac. Sci. Technol. B Microelectron. Nanom. Struct.* **2006**, *24* (6), 2523−2532.
(56) Kim, W. D.; Hwang, G. W.; Kwon, O. S.; Kim, S. K.; Cho, M.; Jeong, D. S.; Lee, S. W.; Seo, M. H.; Hwang, C. S.; Min, Y.-S.; Cho, Y. J. Growth Characteristics of Atomic Layer Deposited TiO2 Thin Films on Ru and Si Electrodes for Memory Capacitor Applications. *J. Electrochem. Soc.* **2005**, *152* (8), C552−C559.
(57) Sinha, A.; Hess, D. W.; Henderson, C. L. A Top Surface Imaging Method Using Area Selective ALD on Chemically Amplified Polymer Photoresist Films. *Electrochem. Solid-State Lett.* **2006**, *9* (11), G330−G333.
(58) Lim, J. W.; Yun, S. J.; Lee, J. H. Characteristics of TiO2 Films Prepared by ALD With and Without Plasma. *Electrochem. Solid-State Lett.* **2004**, *7* (11), F73−F76.
(59) Seo, E. K.; Lee, J. W.; Sung-Suh, H. M.; Sung, M. M. Atomic Layer Deposition of Titanium Oxide on Self-Assembled-Monolayer-Coated Gold. *Chem. Mater.* **2004**, *16* (10), 1878−1883.
(60) Xie, Q.; Musschoot, J.; Deduytsche, D.; Van Meirhaeghe, R. L.; Detavernier, C.; Van den Berghe, S.; Jiang, Y.-L.; Ru, G.-P.; Li, B.-Z.; Qu, X.-P. Growth Kinetics and Crystallization Behavior of TiO2 Films Prepared by Plasma Enhanced Atomic Layer Deposition. *J. Electrochem. Soc.* **2008**, *155* (9), H688−H692.
(61) Hamann, T. W.; Martinson, A. B. F.; Elam, J. W.; Pellin, M. J.; Hupp, J. T. Atomic Layer Deposition of TiO2 on Aerogel Templates: New Photoanodes for Dye-Sensitized Solar Cells. *J. Phys. Chem. C* **2008**, *112* (27), 10303−10307.
(62) Park, K. S.; Seo, E. K.; Do, Y. R.; Kim, K.; Sung, M. M. Light Stamping Lithography: Microcontact Printing without Inks. *J. Am. Chem. Soc.* **2006**, *128* (3), 858−865.
(63) Watanabe, T.; Hoffmann-Eifert, S.; Yang, L.; Rüdiger, A.; Kügeler, C.; Hwang, C. S.; Waser, R. Liquid Injection Atomic Layer Deposition of TiOx Films Using Ti[OCH(CH3)2]4. *J. Electrochem. Soc.* **2007**, *154* (6), G134−G140.
(64) Gu, D.; Baumgart, H.; Abdel-Fattah, T. M.; Namkoong, G. Synthesis of Nested Coaxial Multiple-Walled Nanotubes by Atomic Layer Deposition. *ACS Nano* **2010**, *4* (2), 753−758.
(65) Standridge, S. D.; Schatz, G. C.; Hupp, J. T. Toward Plasmonic Solar Cells: Protection of Silver Nanoparticles via Atomic Layer Deposition of TiO2. *Langmuir* **2009**, *25* (5), 2596−2600.
(66) Park, H. H.; Kang, P. S.; Kim, G. T.; Ha, J. S. Effect of Gate Dielectrics on the Device Performance of SnO2 Nanowire Field Effect Transistors. *Appl. Phys. Lett.* **2010**, *96* (10), 102908−1−102908−3.
(67) Qin, Y.; Liu, L.; Yang, R.; Gösele, U.; Knez, M. General Assembly Method for Linear Metal Nanoparticle Chains Embedded in Nanotubes. *Nano Lett.* **2008**, *8* (10), 3221−3225.

DOI: 10.1021/acs.chemmater.7b05128
Chem. Mater. XXXX, XXX, XXX−XXX

(68) Shin, H.; Jeong, D. K.; Lee, J.; Sung, M. M.; Kim, J. Formation of TiO2 and ZrO2 Nanotubes Using Atomic Layer Deposition with Ultraprecise Control of the Wall Thickness. *Adv. Mater.* **2004**, *16* (14), 1197−1200.
(69) Zhang, Z.; Triani, G.; Fan, L. J. Amorphous to Anatase Transformation in Atomic Layer Deposited Titania Thin Films Induced by Hydrothermal Treatment at 120 °C. *J. Mater. Res.* **2008**, *23* (9), 2472−2479.
(70) Lu, J.; Kosuda, K. M.; Van Duyne, R. P.; Stair, P. C. Surface Acidity and Properties of TiO 2/SiO 2 Catalysts Prepared by Atomic Layer Deposition: UV - Visible Diffuse Reflectance, DRIFTS, and Visible Raman Spectroscopy Studies. *J. Phys. Chem. C* **2009**, *113*, 12412−12418.
(71) Puurunen, R. L. Surface Chemistry of Atomic Layer Deposition: A Case Study for the Trimethylaluminum/water Process. *J. Appl. Phys.* **2005**, *97* (12), 1−52.
(72) Bae, C.; Kim, S.; Ahn, B.; Kim, J.; Sung, M. M.; Shin, H. Template-Directed Gas-Phase Fabrication of Oxide Nanotubes. *J. Mater. Chem.* **2008**, *18* (12), 1362−1367.
(73) Ko, C. H.; Lee, W.-J. Formation of Al2O3−TiO2 Bilayer Using Atomic Layer Deposition and Its Application to Dynamic Random Access Memory. *J. Solid State Electrochem.* **2007**, *11* (10), 1391−1397.
(74) Matero, R.; Rahtu, A.; Ritala, M. Effect of Water Dose on the Atomic Layer Deposition Rate of Oxide Thin Films. *Thin Solid Films* **2000**, *368*, 1−7.
(75) Langner, A.; Knez, M.; Müller, F.; Gösele, U. TiO2Microstructures by Inversion of Macroporous Silicon Using Atomic Layer Deposition. *Appl. Phys. A: Mater. Sci. Process.* **2008**, *93* (2), 399−403.
(76) Knez, M.; Kadri, A.; Wege, C.; Gösele, U.; Jeske, H.; Nielsch, K. Atomic Layer Deposition on Biological Macromolecules: Metal Oxide Coating of Tobacco Mosaic Virus and Ferritin. *Nano Lett.* **2006**, *6* (6), 1172−1177.
(77) Mueller, R.; Kammler, H. K.; Wegner, K.; Pratsinis, S. E. OH Surface Density of SiO2 and TiO2 by Thermogravimetric Analysis. *Langmuir* **2003**, *19* (1), 160−165.
(78) Elliott, S. D.; Greer, J. C. Simulating the Atomic Layer Deposition of Alumina from First Principles. *J. Mater. Chem.* **2004**, *14* (21), 3246−3250.
(79) Kim, S.; Choi, G.; Kim, J.; Hwang, C. Growth Behavior of Al-Doped TiO2 Thin Films by Atomic Layer Deposition. *Chem. Mater.* **2008**, *20* (11), 3723−3727.

DOI: 10.1021/acs.chemmater.7b05128
Chem. Mater. XXXX, XXX, XXX−XXX